Available online at www.sciencedirect.com
SCIENCE DIRECT®
PERGAMON
International Journal of Heat and Mass Transfer 46 (2003) 3051–3059
International Journal of HEAT and MASS TRANSFER
www.elsevier.com/locate/ijhmt

Effect of tube alignment on the heat/mass transfer from a plate fin and two-tube assembly: naphthalene sublimation results

Jin-Yoon Kim, Tae-Ho Song *

Department of Mechanical Engineering, Korea Advanced Institute of Science and Technology, Kusong-dong 373-1, Yusong-gu, Taejon, South Korea

Received 10 July 2002; received in revised form 16 December 2002

Abstract

Flow and heat/mass transfer in a plate fin and two-tube assembly is examined using the naphthalene sublimation technique. The examined parameter is the offset of two-tube centers to tube diameter ratio s/D for two Reynolds numbers Re_D: 1770 and 2660.

The local heat/mass transfer coefficient is always large at the leading edge of the plate and also in front of the tube. The horseshoe vortex formed in front of the first tube increases the local heat/mass transfer rate not only around the first tube itself but also around the second tube. The total heat/mass transfer rate from the plate increases with s/D and it reaches a saturation beyond $s/D = 0.5$. Similar behavior is observed for the pressure drop, showing that $s/D \cong 0.5$ is the optimal offset for the tested range. When the Reynolds number is as high as 2660, the effect of tube offset is significant, so that the total heat/mass transfer rate from the plate for the two-row tube case is larger than that for a single tube case.

1. Introduction

Due to its durability and productivity, plate fins/circular tube assembly is used extensively in various thermal engineering applications, for example, in air conditioning units, process gas heaters and coolers, compressor inter- and after-coolers, etc. Since it has a simple geometry, many researcher groups have examined its performance in various ways.

Saboya and Sparrow [1] use the naphthalene mass transfer method to measure the local coefficients for two-row plate-finned tube heat exchangers for $\delta/D = 0.193$ and $s/D = 1.25$. They report that the effect of developing boundary layers is nearly negligible at the second row of tubes and the vortex system is the main factor to increase the mass transfer rate at the second row. They also report that the local peak transfer rate due to the vortex system in front of the second row is 50% greater than that of the first row when the Reynolds number based on tube diameter is about 2500. However, no extensive search for the optimal tube staggering is made. Tsai and Sheu [2] study the complicated vortex behavior in a two-row finned tube heat exchanger by using a three-dimensional numerical code. They give a highly detailed view of the physical processes, but do not explain the interaction between the two vortex systems around each of the two rows, probably because the Reynolds numbers simulated in their calculations are very low. Jang et al. [3] numerically simulate the similar assembly with increased number of tube rows. Their study shows that the Nusselt number decreases when the number of tube rows increases and it approaches an asymptotic value when the number of tube rows is greater than 4. Onishi et al. [4] also examine numerically the heat transfer from a two-row plate-finned tube heat exchanger. They report that the tube-to-tube conduction effect is very important in their tested case.

* Corresponding author. Tel.: +82-42-869-3032; fax: +82-42-869-3210.
E-mail address: thsong@kaist.ac.kr (T.-H. Song).

0017-9310/03/$ - see front matter © 2003 Elsevier Science Ltd. All rights reserved.
doi:10.1016/S0017-9310(03)00091-7

Nomenclature

D	disk diameter (fixed at 20 mm)
D_N	diffusion coefficient of naphthalene in air [m^2/s]
Gr_{Lm}	the Grashof number ($\equiv (\rho_{sat}/\rho_{air})gL_m^3/\nu^2$)
f	friction factor ($\equiv 2\Delta p\delta/\rho_{air}U^2L$)
g	gravitational acceleration (9.8 m/s^2)
h_m	mass transfer coefficient [m/s]
k	thermal conductivity [W/m K]
L	length of test section (fixed at 120 mm)
l	x-coordinates of tube center location [m]
L_m	mean length of test section ($\equiv 2LW/(L+W)$)
$\dot{m}''$	sublimation mass flux [kg/m^2 s]
$\dot{M}$	total mass flow rate of sublimated naphthalene [kg/s]
$\dot{Q}$	volume flow rate of air [m^3/s]
Re_D	the Reynolds number ($\equiv UD/\nu$)
s	the offset length of two-tube centers [m]
Sc	the Schmidt number
Sh_D	the Sherwood number ($\equiv h_mD/D_N$)
U	bulk velocity of air [m/s]
W	span of test section (fixed at 100 mm)
x	coordinates along the air flow [m]
y	coordinates transverse to the air flow [m]
z	vertical coordinates [m]

Greek symbols

δ	gap size between two plates (fixed at 4 mm)
τ	naphthalene sublimation depth [m]
τ_{nc}	naphthalene sublimation depth by natural convection [m]
ν	kinematic viscosity of air [m^2/s]
ρ_s	density of solid naphthalene [kg/m^3]
ρ_{sat}	saturation density of naphthalene vapor [kg/m^3]
ρ_{bulk}	bulk density of naphthalene in the air [kg/m^3]

Until now, however, reported results about the quantitative effect of the tube offset between the two-tube centers on heat transfer rate are rarely found. The authors have demonstrated the applicability of naphthalene sublimation technique in their prior publication [5], where they find the optimal position of a single tube in a plate fin as the most downstream. This paper is to find the optimal offset for a two-tube case using the same experimental technique. It is intended to scrutinize the microscopic flow and heat transfer phenomenon as well as to evaluate the overall performance to find out the optimal offset. Test of pressure loss is also performed.

2. Experimental method using naphthalene sublimation technique

2.1. Test section and apparatus

A schematic of the test section is shown in Fig. 1. Two plates are $130 \times 130 \times 10(t)$ mm^3, and made of stainless steel. Inside the surface of each plate is covered with molded naphthalene, which has the size of $100(W) \times 120(L) \times 2(t)$ mm^3. Circular acrylic disks are used to simulate the tubes. They are 20 mm in diameter and are pasted on the naphthalene surface. It thus corresponds to a heat transfer problem where the fin efficiency is 100% while the heat transfer from the tube is not accounted for. The gap size is controlled by the thickness δ of the Teflon spacers and the disks. Effect of the spacer on the overall flow is considered to be negligible except near the spacer itself where the wall effect is evidently exerting to the order of the gap size. The examined gap size is fixed at 4 mm. During the sublimation experiment, the test section is completely sealed and immersed in a water bath. The water is vigorously agitated and it is connected to a constant temperature water circulator to maintain a uniform temperature.

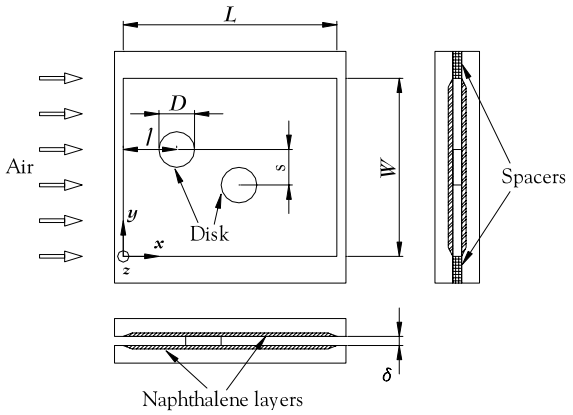

Fig. 1. Schematic of the test section.

Fig. 2 shows a schematic diagram of the experimental apparatus. Dry air is supplied from an air bomb through pressure regulators. To control the volume flow rate of air accurately, the volume flow rate of air is measured by a laminar-flowmeter which consists of a electronic micro-manometer(max. 200 Pa) and 12 tubes of 4 mm

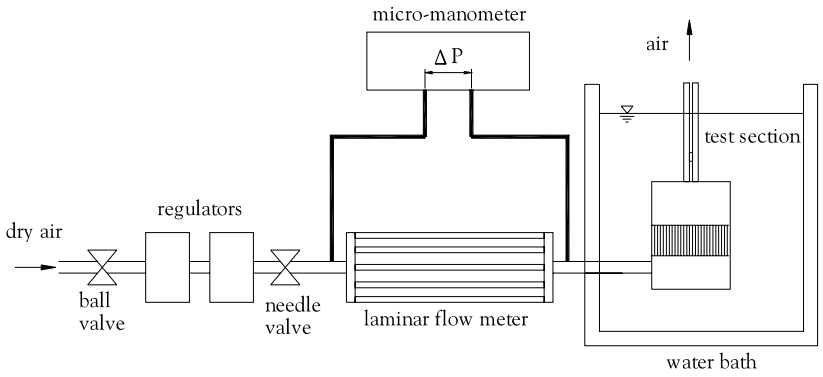

Fig. 2. Schematic diagram of the experimental apparatus.

inner diameter and 500 mm length. The airflow inside the tubes is perfectly laminar so that the theoretical Hagen–Poiseuille flow rate prediction is almost identical with actual calibration result using a bubble meter. The vapor pressure of naphthalene is known to be very sensitive to temperature. At room temperature, it varies about 10% per °C. This is why the test section temperature is accurately maintained by using the aforementioned water bath and circulator.

The pressure drop is measured using multiple of pressure holes near $x = 0$ and $x = L$. Each spanwise average pressure measured at the up- and downstream is taken to convert to the skin friction factor f.

The schematic diagram of the sublimated naphthalene depth measurement system is shown in Fig. 3. It consists of a two-axis auto-traverse system, a depth gauge (LVDT) along with a data acquisition card and a personal computer for data storage and reduction. The two-axis auto-traverse system has step motors with a resolution of 1.8° per step (0.02 mm in linear direction). The depth gauge has range of ±0.508 mm and linearity error of 0.170%. The total resolution of the LVDT and the analog-to-digital card is 0.25 μm and the sublimation depth uncertainty of the entire measurement system is about 1 μm.

2.2. Procedure and data processing

The detailed description of the experimental procedure is available in the authors' prior paper [5]. Here, only a brief description is given.

Reagent grade (99% pure) naphthalene crystals are molded onto the plates. Before and after blowing air over the naphthalene plates, they are scanned by the depth measurement system. The scanning area is $100(x) \times 60(y)$ mm^2 and scanned points are 1 mm apart in both of the longitudinal and transverse directions. The total scanning time is about 40 min. In the blowing

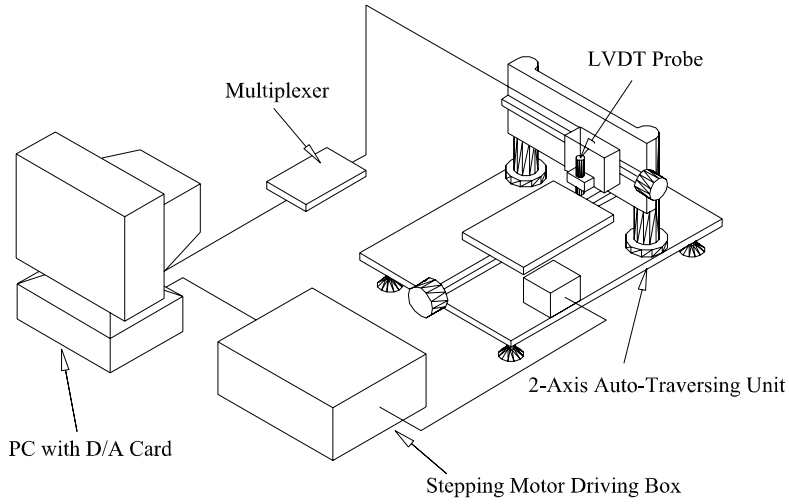

Fig. 3. Schematic diagram of the sublimated depth measurement system.

time, the plates are assembled and the whole assembly is immersed in the water bath. The total blowing time is from 90 to 150 min, which is varied considering the competing two effects, i.e., the increase of signal to noise ratio of the depth measuring system and the decrease of distortion of geometry $d\delta/\delta$ at large blowing time. In this experiment, the maximum $d\delta/\delta$ is retained within 0.038.

The local sublimation depth is calculated from the change of surface elevation before and after the blowing. Then the local mass flux $\dot{m}''$ at each location is calculated using the following expression,

$$\dot{m}''(x,y) = \rho_s \frac{\tau(x,y)}{\Delta t}, \tag{1}$$

where ρ_s is the density of solid naphthalene, τ is the local sublimation depth, and Δt is the blowing time. Thermophysical properties of naphthalene are obtained from Goldstein and Cho [6]. The local mass transfer coefficient h_m can then be calculated as follows,

$$h_m(x,y) = \frac{\dot{m}''(x,y)}{\rho_{sat} - \rho_{bulk}(x)}, \tag{2}$$

where ρ_{sat} is the saturation vapor density of naphthalene and it represents the density of naphthalene vapor at the wall. It is obtained from the perfect gas law using the saturated vapor pressure (as recommended by Goldstein and Cho [6]). And ρ_{bulk} is the bulk density of naphthalene vapor in the local airflow passing through the cross-section at a fixed x-coordinate. It can be evaluated as

$$\rho_{bulk}(x) = \rho_{bulk}(0) + \frac{\dot{M}(x)}{\dot{Q}}, \tag{3}$$

where $\dot{Q}$ is the volume flow rate of air passing through the test section and $\dot{M}$ is the rate of total mass transfer from both of the plates between 0 to x in the x-direction, and 0 to W (span of the naphthalene mold) in the y-direction. Since $\rho_{bulk}(0) = 0$ and $\dot{M}(x)$ is given by (note that we have two naphthalene surfaces, up and down),

$$\dot{M}(x) = 2\int_0^x \int_0^W \dot{m}''(x,y)\,dy\,dx, \tag{4}$$

the local mass transfer coefficient h_m is finally expressed as

$$h_m(x,y) = \frac{\dot{m}''(x,y)}{\rho_{sat} - \frac{2}{\dot{Q}}\int_0^x \int_0^W \dot{m}''(x,y)\,dy\,dx}. \tag{5}$$

The local Sherwood number Sh_D is then calculated by

$$Sh_D = \frac{h_m D}{D_N}, \tag{6}$$

where D_N is the binary diffusion coefficient for naphthalene vapor in air.

When obtaining the local mass flux $\dot{m}''$, the natural convective mass transfer during the scanning period must be considered. To calculate the sublimation depth during the scanning time, the following empirical correlation obtained from heat transfer from a cold surface facing upward is used for the average Sherwood number [7],

$$\overline{Sh}_{Lm} = 0.27(Gr_{Lm}Sc)^{1/4}, \tag{7}$$

where the Grashof number Gr_{Lm} and the mean length L_m of test section are defined as,

$$Gr_{Lm} \equiv \frac{(\rho_{sat}/\rho_{air})gL_m^3}{\nu^2}, \tag{8}$$

$$L_m \equiv \frac{2LW}{L+W}. \tag{9}$$

The obtained mass transfer coefficient h_m is used to compute the sublimation depth τ_{nc} by natural convection from the following equation,

$$\tau_{nc} = \frac{h_m(\rho_{sat} - \rho_\infty)\Delta t}{\rho_s}, \tag{10}$$

where the naphthalene density in the free space ρ_∞ is zero indeed, and Δt is a scanning time (usually about 40 min). Note that the real sublimation time in the depth measurement system between the pre- and post-experiment measurements is Δt for each measuring point, since the two scanning procedures are exactly repeated from a fixed starting corner to an ending corner. To confirm Eq. (10), a naphthalene layer is freely exposed to air for 24 h and the sublimation depth is measured. The measurement and the prediction both give about 18 μm of sublimation depth within roughly 10% error against each other. Consequently, the sublimation depth by natural convection is about 0.5 μm for 40 min. This is subtracted from the raw sublimation depth measurement. Note that the error in τ_{nc} is about 0.05 μm while the depth measurement by the LVDT is about 4% (for typical sublimation depth of 20 μm or more, this corresponds to error of more than 0.8 μm). Consequently, the error in τ_{nc} is negligibly small compared with the other major measurement errors. In this study, both local and span-averaged results are presented. Span averaging is done by simply taking the arithmetic mean of the central 60 data points at 1 mm interval in the y-direction.

The uncertainty of the Sherwood number given by Eq. (6) can be evaluated from [8],

$$\left(\frac{dSh_D}{Sh_D}\right)^2 = \left(\frac{dD_N}{D_N}\right)^2 + \left(\frac{dh_m}{h_m}\right)^2. \tag{11}$$

In this experiment, the uncertainty in the diffusion coefficient D_N is 4.1% [6]. Considering the complicated

expression of h_m in Eq. (5), the uncertainty dh_m can be expressed as,

$$\left(\frac{dh_m}{h_m}\right)^2 = \left(\frac{d\tau}{\tau}\right)^2 + \left(\frac{\rho_{bulk}}{\rho_{sat}-\rho_{bulk}}\frac{d\dot{Q}}{\dot{Q}}\right)^2 + \left(\frac{\rho_{sat}}{\rho_{sat}-\rho_{bulk}}\frac{d\rho_{sat}}{\rho_{sat}}\right)^2 + \left(\frac{\rho_{bulk}}{\rho_{sat}-\rho_{bulk}}\frac{d\rho_s}{\rho_s}\right)^2. \quad (12)$$

In the far downstream region, the above uncertainty reaches a maximum since ρ_{bulk} approaches ρ_{sat} indefinitely. By using the data of that region, the uncertainties in $\tau, \dot{Q}$, ρ_{sat} and ρ_s are 4%, 4.5%, 3.9% and 1.1% respectively. The magnification factors $\rho_{bulk}/(\rho_{sat}-\rho_{bulk})$ and $\rho_{sat}/(\rho_{sat}-\rho_{bulk})$ are then 0.77 and 1.77 respectively. Comprising all these uncertainties, the total uncertainty in Sh_D is 8.7%.

3. Results and discussion

In the prior work of Kim and Song [5], the structure of the horseshoe vortex in front of a single tube is well explained. In this study, we focus more on the vortices interaction between the two tubes on the mass transfer rate.

In the experiment, the span to tube diameter ratio W/D is fixed at 5.0, the length to span ratio L/W is also fixed at 1.2 and the gap to diameter ratio δ/D is taken as 0.2. Typical application of fin/tube assembly for domestic air conditioners shows tube diameter of less than 10 mm and air velocity of a few m/s. The Reynolds number Re_D is taken as 1770 and 2660, and the tube offset to diameter ratio s/D is extensively varied as 0.0, 0.25, 0.5 and 1.0.

First of all, a typical three-dimensional plot of experimental results with $Re_D = 2660$ (corresponding to $U = 2.1$ m/s), $\delta/D = 0.2$ and $s/D = 0.5$ is illustrated in Fig. 4. In this figure, we can find that the mass transfer rate is very high in front of the tubes as well as at the leading edge of the plate where the boundary layer is beginning to develop. These characteristics are the same as has been mentioned by Saboya and Sparrow [1] and they are the same as in the single tube case studied in the previous report [5]. The small subsidiary horseshoe vortex attached in front of the main vortex is also found in the figure. As mentioned by Kim and Song [5] for a single tube case, the high mass transfer rate in front of the tube is due to the horseshoe vortex. However, in the case of two-row tubes, the horseshoe vortex behaves in a complicated manner. The wake size behind the first tube is reduced and the horseshoe vortex beside the second tube is magnified. These facts are further explained by the following figures.

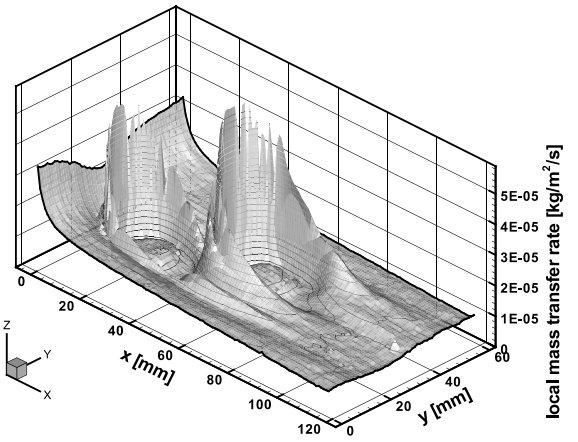

Fig. 4. A typical 3-D plot of the local mass transfer rate at $Re_D = 2660$ and $s/D = 0.5$.

Figs. 5 and 6 are two-dimensional contour plots of local mass transfer rate at the two tested Reynolds numbers and at various s/D. In these series of figures, the mass transfer rate around the second tube is found to increase with the tube offset. Increase of the tube offset causes increase of the airflow rate through the passage between the two tubes, and as the result, it causes an increase of the mass transfer rate there. In Figs. 5(a) and 6(a) (in-line alignment), the formation of horseshoe vortex in front of the second tube is nearly negligible because the second tube is placed in the wake region of the first tube. When the tube offset s is increased to 5 mm as in Figs. 5(b) and 6(b), the airflow rate between the two tubes is increased and a horseshoe vortex in front of the second tube is built. However, the horseshoe vortex extends its trail around only the half side of the second tube. When s is further increased to 10 mm (Figs. 5(c) and 6(c)), the horseshoe vortex in front of the second tube is further developed and wraps around it entirely. It is important to note that the horseshoe vortex developed in front of the first tube interacts with that of the second tube to result in a high mass transfer rate in a large area beside the second tube, especially at high Re_D. When Re_D is as high as 2660, it is considered that the vortex shedding behind the first tube intensifies the interaction between the two horseshoe vortices and, as the result, the mass transfer rate in this region is locally very high. When s is further increased to 20 mm as in Figs. 5(d) and 6(d), the airflow between two tubes can pass freely and therefore the interaction between two horseshoe vortices is almost negligible so that the airflows around the two tubes are almost independent of each other and are very similar to that of the single tube case.

To show the overall results quantitatively, the span-averaged Sherwood number with various tube offset is plotted in Fig. 7. It has the lowest in the in-line

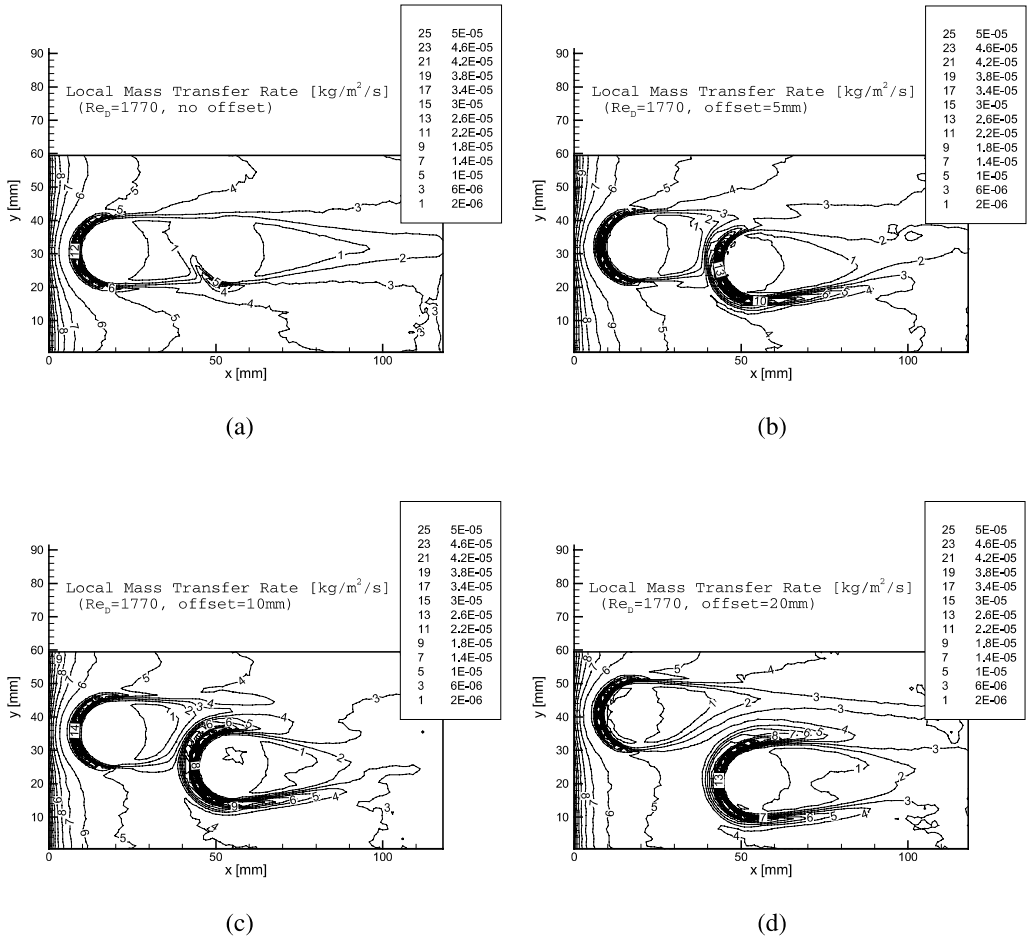

Fig. 5. 2-D contour plots of local mass transfer rate with various tube offset length at $Re_D = 1770$: (a) $s/D = 0$, (b) $s/D = 0.25$, (c) $s/D = 0.5$, (d) $s/D = 1$.

arrangement at the two Reynolds numbers. It increases with the increase of the tube offset due to the aforementioned vortex interactions. At the tube offset of 5 mm (corresponding to $s/D = 0.25$), the local Sherwood number is very large in front of the second tube because the airflow impinges on the head of the second tube. Nevertheless, it is still low behind the second tube because the space between two tubes is not large enough for airflow to pass freely. When the tube offset is increased beyond 10 mm, the interaction between the horseshoe vortices is intensified and the Sherwood number in front of and behind the second tube is increased also. Especially when the Reynolds number is 2660, the effect of vortex shedding from the first tube intensifies the interaction of horseshoe vortices and decreases the size of wake behind the first tube. As the result, the local Sherwood number behind the second tube is larger than that of the single row tube case. In contrast, when $Re_D = 1770$ as shown in Fig. 7(a), the vortex shedding effect is too weak to increase the local Sherwood number beyond the level of the single row tube case. Also note that, when the tube offset is increased from 10 to 20 mm, no further increase of Sherwood number is made. Furthermore, when $Re_D = 1770$, the Sherwood number around and behind the second tube is somewhat lowered from the case of 10 mm tube offset. It is considered to be due to the existence of sustained wake from the first tube to the outlet. Saboya and Sparrow [1] also confirm this results in that mass transfer rate of one-row tube case is larger than that of two-row tube case when the Reynolds number is small with $\delta/D = 0.193$ and $s/D = 1.25$. Fig. 8 concisely shows the effect of the tube offset on the total mass transfer rate. Note that the mass transfer area of the two-tube case is smaller than that of the one-tube case by a tube cross-sectional area. Nevertheless, it is shown that the total mass transfer rate of the two-tube case can be greater. When $Re_D = 1770$, the total mass transfer

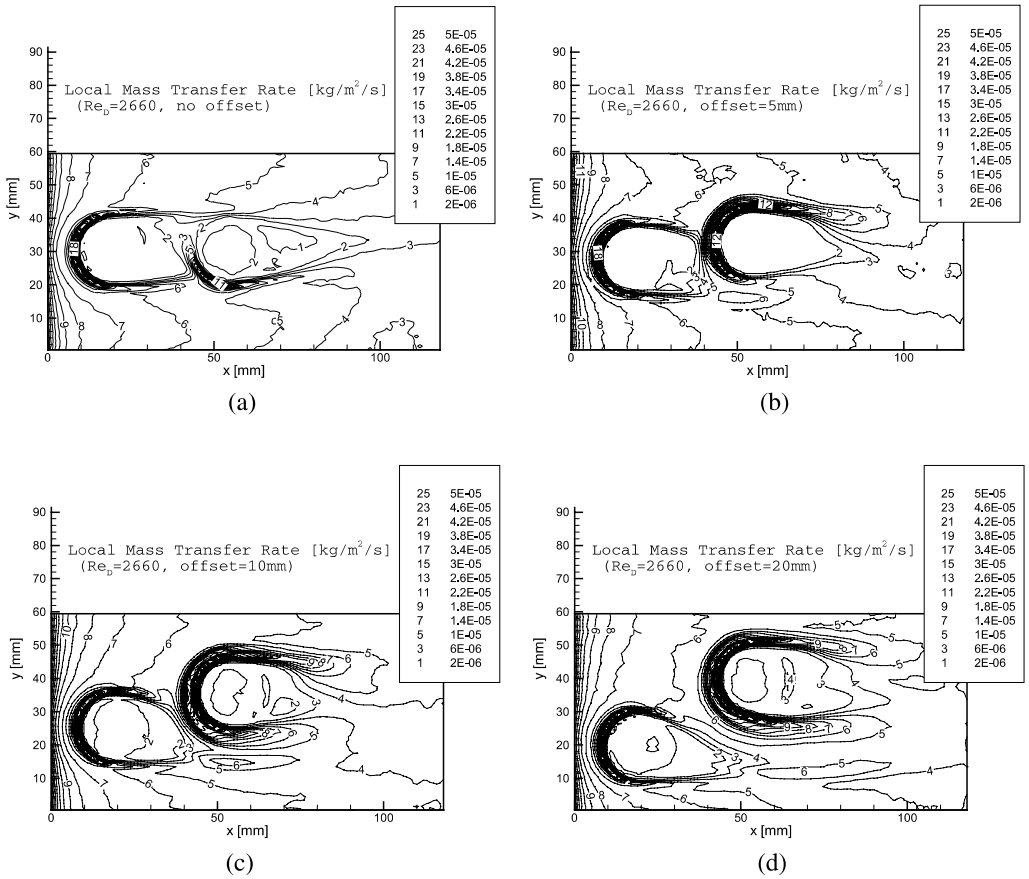

Fig. 6. 2-D contour plots of local mass transfer rate with various tube offset length at $Re_D = 2660$: (a) $s/D = 0$, (b) $s/D = 0.25$, (c) $s/D = 0.5$, (d) $s/D = 1$.

rate from the plate with the two-row tubes is less than that of a single row tube (compare the solid circles with the hollow ones) in all set of the tube offsets. But when $Re_D = 2660$, the total mass transfer rate with $s/D > 0.5$ is larger than that of the single row tube case (compare again the solid rectangles with the hollow ones). And further increase of s/D beyond 1.0 does not increase the total mass transfer rate further in any Reynolds number.

Fig. 9 shows the friction factor f as defined by,

$$\Delta p = f \frac{\rho_{air} U^2}{2} \frac{L}{\delta}, \tag{13}$$

where Δp is the total pressure drop from $x = 0$ to L. The solid line is for the case of a fully developed laminar flow between two parallel plates without disk. The analytic exact expression for this case shows that f is inversely proportional to Re_D, i.e. [9],

$$f = \frac{24}{Re_D} \frac{D}{\delta}. \tag{14}$$

As can be found from the graph, the value of the experimental friction factor without a disk is found to be greater than the theoretical value. It is considered that the developing boundary layer near the leading edge of the plate exhibits greater skin friction than the fully developed case. This characteristic feature is more distinguished when the Reynolds number is greater so that the entrance length is larger. Also, the friction factor with disks is greater than that without disks, which is quite in agreement with our intuition. Also, the friction factor is roughly inversely proportional to Re_D. This means that the flow is almost laminar so that the pressure drop is mostly caused by skin friction.

The friction factor f shows a similar trend as the total mass transfer rate, i.e., it increases almost linearly from $s/D = 0$ to $s/D = 1.0$ and remains nearly constant thereafter. The increase of f is because the surface area with high velocity gradient, and thus total skin friction, is increased. Consequently, the optimal s/D is found to be about 0.5 for the tested range of parameters.

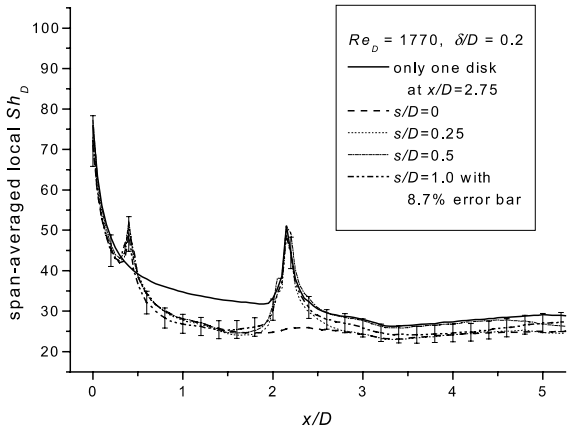

(a)

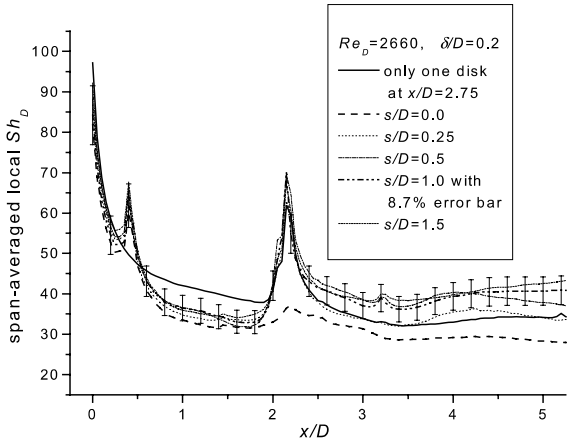

(b)

Fig. 7. Span-averaged Sh_D along the longitudinal direction with various offset of two-tube centers: (a) $Re_D = 1770$, (b) $Re_D = 2660$.

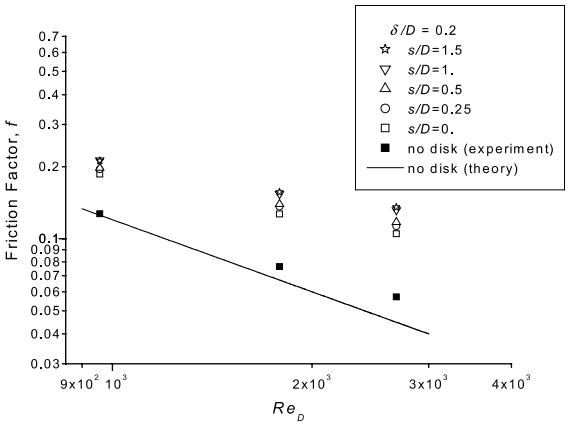

Fig. 9. Effect of the offset of two-tube centers on friction factor.

4. Conclusion

To investigate the microscopic flow and heat/mass transfer phenomenon and also to evaluate the overall performance to find out the optimal tube offset of two-row tubes, the local mass transfer coefficient on the plate is scrutinized from the measurement of sublimated naphthalene depth.

The local mass transfer rate is large at the leading edge of the plate and also in front of the tubes in all of the examined cases. The horseshoe vortices formed in front of the tubes cause significant increase in the total heat/mass transfer rate. It is found that the staggered tube arrangement gives greater heat/mass transfer rate than the in-line tube arrangement. This is since the horseshoe vortex formed in front of the first tube extends to the second tube and thus increases the local heat/mass transfer rate around the second tube. How-

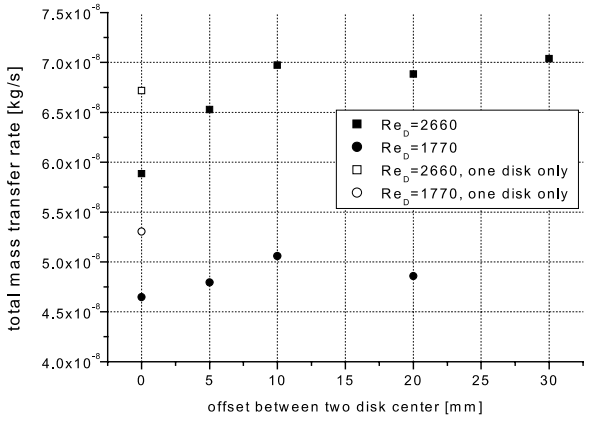

Fig. 8. Effect of the offset of two-tube centers on total mass transfer rate.

ever, no further increase in the total heat/mass transfer rate is observed when s/D is increased beyond 0.5. The friction factor shows similar behavior with the total heat/mass transfer rate. Consequently, the optimal s/D is found to be about 0.5 for the tested range of parameters.

Acknowledgement

This work has been supported by the Critical Technology of the Ministry of Science and Technology, Korea.

References

[1] F.E.M. Saboya, E.M. Sparrow, Transfer characteristics of two-row plate fin and tube heat exchanger configurations, Int. J. Heat Mass Transfer 19 (1976) 41–49.

[2] S.F. Tsai, T.W.H. Sheu, Some physical insights into a two-row finned-tube heat transfer, Comput. Fluids 27 (1) (1998) 29–46.

[3] J.Y. Jang, M.C. Wu, W.J. Chang, Numerical and experimental studies of three-dimensional plate-fin and tube heat exchangers, Int. J. Heat Mass Transfer 39 (14) (1996) 3057–3066.

[4] H. Onishi, K. Inaoka, K. Matsubara, K. Suzuki, Numerical analysis of flow and conjugate heat transfer of a two-row plate-finned tube heat exchanger, in: Proceedings of the Second International Conference on Compact Heat Exchangers and Enhancement Technology for the Process Industries, Banff, 1999, pp. 175–182.

[5] J.-Y. Kim, T.-H. Song, Microscopic phenomena and macroscopic evaluation of heat transfer from plate fins/circular tube assembly using naphthalene sublimation technique, Int. J. Heat Mass Transfer 45 (16) (2002) 3397–3404.

[6] R.J. Goldstein, H.H. Cho, A review of mass transfer measurements using naphthalene sublimation, Exp. Thermal Fluid Sci. 10 (1995) 416–434.

[7] F.P. Incropera, D.P. DeWitt, Fundamentals of Heat and Mass Transfer, third ed., John Wiley & Sons, New York, 1990.

[8] J.P. Holman, Experimental Methods for Engineers, sixth ed., McGraw-Hill, New York, 1994.

[9] F.M. White, Viscous Fluid Flow, second ed., McGraw-Hill, New York, 1991.